

Channel Hardening-Exploiting Message Passing (CHEMP) Receiver in Large-Scale MIMO Systems

T. Lakshmi Narasimhan and A. Chockalingam
 Department of ECE, Indian Institute of Science, Bangalore

Abstract—In this paper, we propose a multiple-input multiple-output (MIMO) receiver algorithm that exploits *channel hardening* that occurs in large MIMO channels. Channel hardening refers to the phenomenon where the off-diagonal terms of the $\mathbf{H}^T \mathbf{H}$ matrix become increasingly weaker compared to the diagonal terms as the size of the channel gain matrix \mathbf{H} increases. Specifically, we propose a message passing detection (MPD) algorithm which works with the real-valued matched filtered received vector (whose signal term becomes $\mathbf{H}^T \mathbf{H} \mathbf{x}$, where \mathbf{x} is the transmitted vector), and uses a Gaussian approximation on the off-diagonal terms of the $\mathbf{H}^T \mathbf{H}$ matrix. We also propose a simple estimation scheme which directly obtains an estimate of $\mathbf{H}^T \mathbf{H}$ (instead of an estimate of \mathbf{H}), which is used as an effective channel estimate in the MPD algorithm. We refer to this receiver as the *channel hardening-exploiting message passing (CHEMP)* receiver. The proposed CHEMP receiver achieves very good performance in large-scale MIMO systems (e.g., in systems with 16 to 128 uplink users and 128 base station antennas). For the considered large MIMO settings, the complexity of the proposed MPD algorithm is almost the same as or less than that of the minimum mean square error (MMSE) detection. This is because the MPD algorithm does not need a matrix inversion. It also achieves a significantly better performance compared to MMSE and other message passing detection algorithms using MMSE estimate of \mathbf{H} . We also present a convergence analysis of the proposed MPD algorithm. Further, we design optimized irregular low density parity check (LDPC) codes specific to the considered large MIMO channel and the CHEMP receiver through EXIT chart matching. The LDPC codes thus obtained achieve improved coded bit error rate performance compared to off-the-shelf irregular LDPC codes.

Keywords – Large-scale MIMO systems, channel hardening, message passing, detection, channel estimation, decoding.

I. INTRODUCTION

Wireless communication systems using multiple-input multiple-output (MIMO) configurations with a large number of antennas have attracted a lot of research attention [1],[2],[3],[4]. These systems can achieve high spectral and power efficiencies. An emerging architecture for large-scale multiuser MIMO communications is one where each base station (BS) is equipped with a large number of antennas and the user terminals are equipped with one antenna each. A key requirement on the uplink (user terminal to BS link) in such large-scale MIMO systems is to achieve reduced channel estimation, detection and decoding complexities at the BS receiver to enable practical implementation, while maintaining good performance. When the number of BS antennas is much larger than the number of uplink users (i.e., low system loading factors), linear detectors like the

minimum mean square error (MMSE) detector are good in terms of both complexity and performance [5]. In the recent years, several low complexity detection algorithms which achieve near-optimal performance in large dimensions using complexities comparable to that of MMSE detection have been proposed [1],[2],[6]-[16]. These algorithms are based on local search (e.g., likelihood ascent search (LAS) algorithm and variants in [1],[2],[6],[7]), meta-heuristics (e.g., reactive tabu search (RTS) and variants in [8],[9]), message passing techniques (e.g., belief propagation (BP) based algorithms in [11],[12]), lattice reduction techniques (e.g., lattice reduction (LR) aided detectors in [13],[14]), and Monte-Carlo sampling techniques (e.g., Markov chain Monte Carlo (MCMC) algorithms in [15]). Issues related channel estimation and low density parity check codes for large-scale MIMO systems are also being addressed [17],[18].

Message passing on graphical models is a promising low-complexity high-performance approach for signal processing in large dimensions [19]. Decoding of turbo codes and LDPC codes, and equalization/detection [20]-[22] are popular examples of the use of message passing algorithms in communications. In [11], a MIMO detection algorithm based on approximate message passing on a factor graph is presented. The message passing algorithm in [12] uses a different approach. It obtains a tree that approximates the fully-connected MIMO graph and performs message passing on this tree.

In this this paper, we propose a promising low-complexity receiver for large-scale MIMO systems. The receiver is based on message passing. The novelty in the proposed receiver lies in the exploitation of the ‘channel hardening’ phenomenon that occurs in large MIMO channels [23],[24],[25],[26]. Channel hardening refers to the phenomenon where the off-diagonal terms of the $\mathbf{H}^T \mathbf{H}$ matrix become increasingly weaker compared to the diagonal terms as the size of the channel gain matrix \mathbf{H} increases. We exploit this for the purposes of detection and channel estimation. The proposed receiver, referred to as the *channel hardening-exploiting message passing (CHEMP)* receiver, consists of two components; a message passing detection (MPD) algorithm and an estimation scheme to obtain an estimate of $\mathbf{H}^T \mathbf{H}$. The highlights of our contributions in this paper can be summarized as follows:

- proposal of the MPD algorithm which works with the real-valued matched filtered received vector, and uses a Gaussian approximation on the off-diagonal terms of

the $\mathbf{H}^T \mathbf{H}$ matrix.

- proposal of a simple estimation scheme which directly obtains an estimate of $\mathbf{H}^T \mathbf{H}$ (instead of an estimate of \mathbf{H}), which is used as an effective channel estimate in the MPD algorithm.
- less than the MMSE detection complexity (because matrix inversion is not needed in the MPD algorithm).
- significantly better performance compared to MMSE and other message passing detection algorithms which use MMSE estimate of \mathbf{H} .
- convergence analysis of the MPD algorithm which proves the existence of a fixed point in the MPD algorithm.
- analysis of the mean square difference of the log-likelihood ratios (LLRs) in the proposed receiver with perfect and estimated channel state information (CSI).
- design of optimized irregular LDPC codes specific to the considered large MIMO channel and the CHEMP receiver through EXIT chart matching.

The rest of the paper is organized as follows. The system model and the channel hardening phenomenon are described in Section II. The proposed CHEMP receiver, and its performance and complexity are presented in Section III. An analysis of the CHEMP receiver is presented in Section IV. Section V presents an extension to higher-order QAM. The design and performance of LDPC codes matched to the large MIMO channel and the CHEMP receiver are presented in Section VI. Conclusions are presented in Section VII.

II. SYSTEM MODEL

Consider a large-scale multiuser MIMO system where K uplink users, each transmitting with a single antenna, communicate with a BS having a large number of receive antennas. Let N denote the number of BS antennas; N is in the range of tens to hundreds. The ratio $\alpha = K/N$ is the system loading factor. We consider $\alpha \leq 1$ (i.e., $K \leq N$). The system model is illustrated in Fig. 1. Each user encodes a sequence of k information bits to a sequence of n coded symbols using an LDPC code of code rate $R = k/n$. The encoded bits are modulated and transmitted. Let \mathbb{A} denote the modulation alphabet. The transmission of one LDPC code block requires $n/(\log_2 |\mathbb{A}|)$ channel uses.

Let $\mathbf{H}_c^{(t)} \in \mathbb{C}^{N \times K}$ denote the channel gain matrix in the t th channel use and $H_{ij}^{(t)}$ denote the complex channel gain from the j th user to the i th BS antenna. The channel gains $H_{ij}^{(t)}$ s are assumed to be independent Gaussian with zero mean and variance σ_j^2 , such that $\sum_j \sigma_j^2 = K$. The σ_j^2 models the imbalance in the received power from user j due to path loss etc., and $\sigma_j^2 = 1$ corresponds to the case of perfect power control. Let $\mathbf{x}_c^{(t)} \in \mathbb{A}^K$ denote the modulated symbol vector transmitted in the t th channel use, where the j th element of $\mathbf{x}_c^{(t)}$ denotes the modulation symbol transmitted by the j th user. Assuming perfect synchronization, the received vector

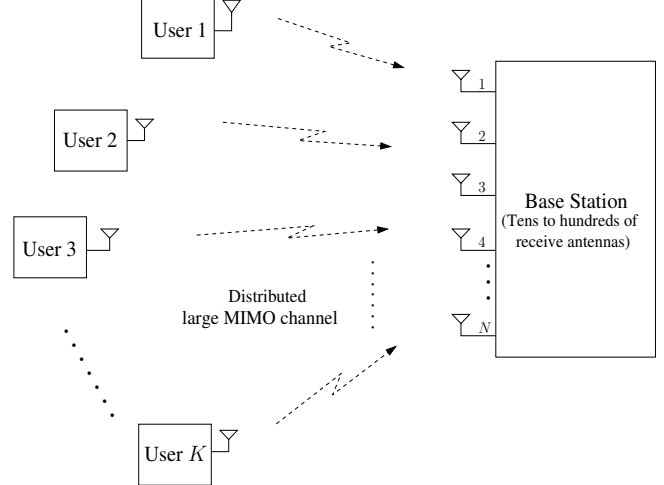


Fig. 1. Large-scale multiuser MIMO system model on the uplink.

at the BS in the t th channel use, $\mathbf{y}_c^{(t)}$, is given by

$$\mathbf{y}_c^{(t)} = \mathbf{H}_c^{(t)} \mathbf{x}_c^{(t)} + \mathbf{w}_c^{(t)}, \quad (1)$$

where $\mathbf{w}_c^{(t)}$ is the noise vector. Dropping the channel use index for convenience, (1) can be written in the real domain as

$$\mathbf{y} = \mathbf{H}\mathbf{x} + \mathbf{w}, \quad (2)$$

where

$$\mathbf{H} \triangleq \begin{bmatrix} \Re(\mathbf{H}_c) & -\Im(\mathbf{H}_c) \\ \Im(\mathbf{H}_c) & \Re(\mathbf{H}_c) \end{bmatrix},$$

$$\mathbf{y} \triangleq \begin{bmatrix} \Re(\mathbf{y}_c) \\ \Im(\mathbf{y}_c) \end{bmatrix}, \quad \mathbf{x} \triangleq \begin{bmatrix} \Re(\mathbf{x}_c) \\ \Im(\mathbf{x}_c) \end{bmatrix}, \quad \mathbf{w} \triangleq \begin{bmatrix} \Re(\mathbf{w}_c) \\ \Im(\mathbf{w}_c) \end{bmatrix},$$

$\Re(\cdot)$ and $\Im(\cdot)$ denote the real and imaginary parts, respectively. Note that $\mathbf{H} \in \mathbb{R}^{2N \times 2K}$, $\mathbf{y} \in \mathbb{R}^{2N}$, $\mathbf{w} \in \mathbb{R}^{2N}$, and $\mathbf{x} \in \mathbb{R}^{2K}$. For a QAM alphabet \mathbb{A} , the elements of \mathbf{x} will take values from the underlying PAM alphabet \mathbb{B} , i.e., $\mathbf{x} \in \mathbb{B}^{2K}$. The elements of \mathbf{w} are modeled as i.i.d. $\mathcal{N}(0, \sigma_n^2)$. The average received SNR per receive antenna is given by $\gamma = \frac{KE_s}{2\sigma_n^2}$, where E_s is the average energy of the transmitted symbols. For the real-valued system model in (2), the maximum-likelihood (ML) detection rule is given by

$$\hat{\mathbf{x}} = \operatorname{argmin}_{\mathbf{x} \in \mathbb{B}^{2K}} (\mathbf{y} - \mathbf{H}\mathbf{x})^T (\mathbf{y} - \mathbf{H}\mathbf{x}). \quad (3)$$

When the transmitted bits are equally likely, then the ML decision rule is same as the maximum a posteriori probability (MAP) decision rule, given by

$$\hat{\mathbf{x}} = \operatorname{argmax}_{\mathbf{x} \in \mathbb{B}^{2K}} \Pr(\mathbf{x} | \mathbf{y}, \mathbf{H}). \quad (4)$$

The exact computation of (3) and (4) requires exponential complexity in K . Message passing algorithms can provide approximate marginalization of the joint distribution in (4) at low complexities. In Section III, we propose such a message passing algorithm, whose novelty lies in exploiting the channel hardening phenomenon that happens in large

MIMO channels. The channel hardening effect in large MIMO channels is described in the following subsection.

A. Channel hardening in large MIMO channels

Channel hardening refers to the phenomenon where the variance of the mutual information of the MIMO channel grows very slowly relative to its mean or even shrink as the number of antennas grows [23]. Consider a $n_r \times n_t$ MIMO channel. As n_r and n_t are increased keeping their ratio fixed, the distribution of the singular values of the MIMO channel matrix becomes less sensitive to the actual distribution of the entries of the channel matrix (as long as the entries are i.i.d.) [24]. This is a result of the Marčenko-Pastur law [25], which states that if the entries of a $n_r \times n_t$ matrix \mathbf{H} are zero mean i.i.d. with variance $1/n_r$, then the empirical distribution of the eigenvalues of $\mathbf{H}^H \mathbf{H}$ converges almost surely, as $n_r, n_t \rightarrow \infty$ with $n_t/n_r = \alpha$, to a density function [26]

$$p_\alpha(x) = \left(1 - \frac{1}{\alpha}\right)^+ \delta(x) + \frac{\sqrt{(x-a)^+(b-x)^+}}{2\pi\alpha x}, \quad (5)$$

where $(x)^+ = \max(x, 0)$, $a = (1 - \sqrt{\alpha})^2$, and $b = (1 + \sqrt{\alpha})^2$. An effect of the Marčenko-Pastur law is that very tall or very wide matrices¹ are very well conditioned. The law also implies that the channel ‘‘hardens’’, i.e., the eigenvalue histogram of a single realization converges to the average asymptotic eigenvalue distribution.

Channel hardening can bring in several advantages in large dimensional signal processing. For example, linear detection in large systems will require inversion of large matrices. Inversion of large random matrices can be done fast using series expansion techniques [27],[28],[29]. Because of channel hardening, approximate matrix inversions using series expansion and deterministic approximations from limiting distribution become effective in large dimensions.

An interesting aspect in channel hardening is that as the size of \mathbf{H} increases, the off-diagonal terms of the $\mathbf{H}^H \mathbf{H}$ matrix become increasingly weaker compared to the diagonal terms, i.e., $\frac{\mathbf{H}^H \mathbf{H}}{n_r} \rightarrow \mathbf{I}_{n_t}$ for $n_r, n_t \rightarrow \infty$ with $n_t/n_r = \alpha$. This phenomenon is pictorially illustrated in Fig. 2, where we have plotted $\mathbf{H}^T \mathbf{H}$ for the real-valued channel model in (2) for 8×8 , 32×32 , 64×64 , and 128×128 channels. In proposing the new receiver algorithm in the next section, we will work with approximations to the off-diagonal terms of the $\mathbf{H}^T \mathbf{H}$ matrix and estimates of $\mathbf{H}^T \mathbf{H}$, which are found to achieve very good performance in large dimensions at low complexities.

III. THE PROPOSED CHEMP RECEIVER

In this section, we present the proposed CHEMP receiver. The proposed CHEMP receiver has two main components: 1) a message passing based detection (MPD) algorithm, and

¹In practice, the channel matrix in a multiuser system with tens of single-antenna users and hundreds of BS antennas will become a very tall matrix on the uplink, and a very wide matrix on the downlink.

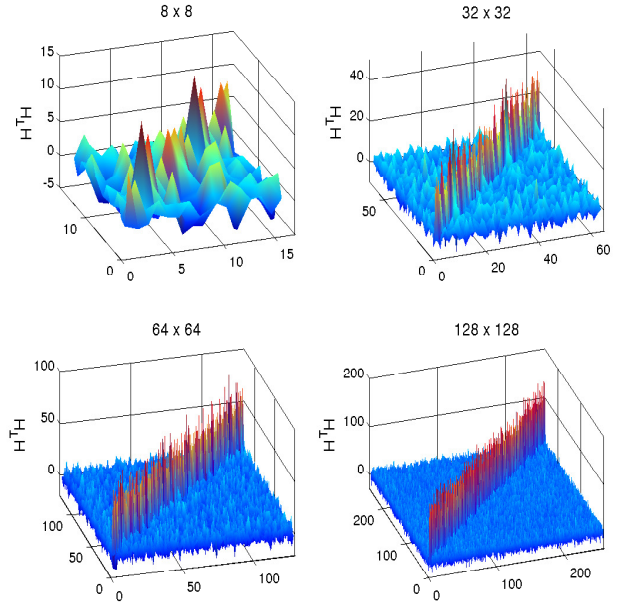


Fig. 2. Magnitude plots of $\mathbf{H}^T \mathbf{H}$ for 8×8 , 32×32 , 64×64 , and 128×128 MIMO channels.

2) a scheme to estimate $\mathbf{H}^T \mathbf{H}$. The proposed MPD algorithm works with the real-valued matched filtered received vector (whose signal term becomes $\mathbf{H}^T \mathbf{H} \mathbf{x}$), and uses a Gaussian approximation on the off-diagonal terms of the $\mathbf{H}^T \mathbf{H}$ matrix. Before we describe the proposed MPD algorithm, we state the following lemma which will be used in the development and analysis of the detection algorithm.

Lemma 1. Let X_i and Y_i be Gaussian random variables with zero mean and variance σ_x^2 and σ_y^2 , respectively. Let $Z_i \triangleq X_i Y_i$ and $Z \triangleq \frac{1}{n} \sum_{i=1}^n Z_i$.

- When X_i and Y_i are independent, $\mathbb{E} Z_i = 0$ and $\mathbb{E} Z_i^2 = \sigma_x^2 \sigma_y^2$. Then by central limit theorem, for large n , $Z \sim \mathcal{N}(0, \frac{\sigma_x^2 \sigma_y^2}{n})$. When X_i and Y_i are i.i.d., $Z \sim \mathcal{N}(0, \frac{\sigma_x^4}{n})$.
- When $X_i = Y_i$, Z is a χ^2 random variable of degree n . $\mathbb{E} Z = \sigma_x^2$ and $\text{Var}(Z) = \frac{2\sigma_x^4}{n}$. \square

A. Proposed MPD algorithm

Consider the real-valued system model in (2). We consider 4-QAM modulation in this section, i.e., $\mathbb{B} = \{\pm 1\}$. We will extend the algorithm to higher-order QAM in Section V. Performing matched filter operation on \mathbf{y} , we have

$$\mathbf{H}^T \mathbf{y} = \mathbf{H}^T \mathbf{H} \mathbf{x} + \mathbf{H}^T \mathbf{w}. \quad (6)$$

From (6), we write the following:

$$\mathbf{z} = \mathbf{J} \mathbf{x} + \mathbf{v}, \quad (7)$$

where

$$\mathbf{z} \triangleq \frac{\mathbf{H}^T \mathbf{y}}{N}, \quad \mathbf{J} \triangleq \frac{\mathbf{H}^T \mathbf{H}}{N}, \quad \mathbf{v} \triangleq \frac{\mathbf{H}^T \mathbf{w}}{N}. \quad (8)$$

The i th element of \mathbf{z} can be written as

$$z_i = J_{ii}x_i + \underbrace{\sum_{j=1, j \neq i}^{2K} J_{ij}x_j + v_i}_{\triangleq g_i}, \quad (9)$$

where J_{ij} is the element in the i th row and j th column of \mathbf{J} , x_i is the i th element of \mathbf{x} , and

$$v_i = \sum_{j=1}^{2N} \frac{H_{ji}w_j}{N} \quad (10)$$

is the i th element of \mathbf{v} , where H_{ji} is the (j, i) th element of \mathbf{H} . Note that the variable g_i defined in (9) denotes the interference-plus-noise term, which involves the off-diagonal elements of $\frac{\mathbf{H}^T \mathbf{H}}{N}$ (i.e., J_{ij} , $i \neq j$). We approximate the g_i term to have a Gaussian distribution with mean μ_i and variance σ_i^2 , i.e., the distribution of g_i is approximated as $\mathcal{N}(\mu_i, \sigma_i^2)$. By central limit theorem, this approximation is accurate for large K, N . The mean and variance in this approximation are given by

$$\mu_i = \mathbb{E}(g_i) = \sum_{j=1, j \neq i}^{2K} J_{ij} \mathbb{E}(x_j) \quad (11)$$

$$\sigma_i^2 = \text{Var}(g_i) = \sum_{j=1, j \neq i}^{2K} J_{ij}^2 \text{Var}(x_j) + \sigma_v^2. \quad (12)$$

Denoting the probability of the symbol x_j as p_j , we have

$$\mathbb{E}(x_j) = (2p_j - 1), \quad \text{Var}(x_j) = 4p_j(1 - p_j). \quad (13)$$

Also, note that by Lemma 1, $\sigma_v^2 = \frac{\sigma_n^2}{2N}$. Because of the above Gaussian approximation, the a posteriori probability (APP) of the symbol x_i can be written as

$$p_i = \Pr(x_i | z_i, \mathbf{J}) \propto \exp\left(\frac{-1}{2\sigma_i^2}(z_i - J_{ii}x_i - \mu_i)^2\right). \quad (14)$$

From (14), the log-likelihood ratio (LLR) of x_i , denoted by L_i , can be written as

$$\begin{aligned} L_i &= \ln \frac{\Pr(z_i | x_i = +1)}{\Pr(z_i | x_i = -1)} \\ &= \frac{2J_{ii}}{\sigma_i^2}(z_i - \mu_i). \end{aligned} \quad (15)$$

From (15), the probability of symbol x_i , can be written as

$$p_i = \frac{e^{L_i}}{1 + e^{L_i}}. \quad (16)$$

Message passing: The system is modeled as a fully-connected graph, where the data symbols in \mathbf{x} represent the nodes. There are $2K$ nodes in the graph corresponding to the $2K$ elements in the vector \mathbf{x} . The i th node uses the knowledge of \mathbf{J} , \mathbf{z} and the incoming APPs $\{p_1, p_2, \dots, p_{i-1}, p_{i+1}, \dots, p_{2K}\}$ to obtain a soft estimate of the interference to symbol x_i , and computes its APP, p_i . That is, each node is an approximate APP processor for its associated symbol, and message passing refers to the

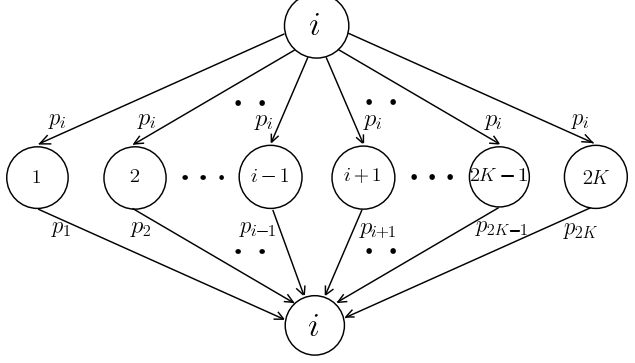


Fig. 3. Message passing in the proposed MPD algorithm.

exchange of APP values computed at each iteration. Figure 3 illustrates the above message passing schedule. Note that the computation of the message p_i in (16) requires the computation of (11), (12) and (15). The algorithm is initialized with $p_i = 0.5, \forall i$, and message passing is carried out for a certain number of iterations, after which the algorithm stops. The values of p_i s at the end are taken as the soft values of x_i s. These soft values can be directly fed to the channel decoder in coded systems. In uncoded systems, a hard estimate of symbol x_i can be obtained as

$$\hat{x}_i = \begin{cases} +1 & \text{if } p_i \geq 0.5 \\ -1 & \text{otherwise.} \end{cases} \quad (17)$$

B. Improving convergence rate

At the end of the t th iteration of the detection algorithm described above, we obtain the probability of the i th user's information bit, p_i^t . The rate of convergence of this sequence $\{p_i^0, p_i^1, p_i^2, \dots, p_i^t, \dots\}$ can be improved by certain techniques. We discuss the following two techniques that helps us to improve the convergence.

- **Aitken acceleration:** Aitken's delta-squared process is a technique known in numerical analysis [30] for accelerating sequence convergence. This method is also used in [22] to accelerate the convergence of the Gaussian belief propagation algorithm. By this method, a linearly converging sequence of real numbers can be accelerated to converge quadratically. Although there is no rigorous proof guaranteeing this rate of convergence, empirical observations have shown that this method does accelerate the convergence of iterative algorithms. According to Aitken's acceleration method, we define a sequence

$$q_i^t = p_i^t - \frac{(p_i^{t+1} - p_i^t)^2}{p_i^{t+2} - 2p_i^{t+1} + p_i^t}. \quad (18)$$

This new sequence q_i^t converges faster than p_i^t and to the same limit, whenever p_i^t converges. After the first three iterations, q_i s can be used as the messages in the algorithm for faster convergence.

- **Damping:** Damping of messages passed in message passing algorithms is a scheme known to improve the

Algorithm 1 Proposed MPD algorithm

Require: \mathbf{z} , \mathbf{J} , σ_v^2 , Δ

- 1: **Initialize:** $p_i^0 \leftarrow 0.5$, $i = 1, \dots, 2K$
- 2: **for** $t = 1$ to *number_of_iterations* **do**
- 3: **for** $i = 1$ to $2K$ **do**
- 4: $\mu_i \leftarrow \sum_{j=1, j \neq i}^{2K} J_{ij} (2p_j^{t-1} - 1)$
- 5: $\sigma_i^2 \leftarrow \sum_{j=1, j \neq i}^{2K} 4J_{ij}^2 p_j^{t-1} (1 - p_j^{t-1}) + \sigma_v^2$
- 6: $L_i \leftarrow \frac{2J_{ii}}{\sigma_i^2} (z_i - \mu_i)$
- 7: $\tilde{p}_i^t \leftarrow \frac{e^{L_i}}{1 + e^{L_i}}$
- 8: **end for**
- 9: $\mathbf{p}^t \leftarrow (1 - \Delta)\tilde{\mathbf{p}}^t + \Delta\mathbf{p}^{t-1}$
- 10: **end for**

rate of convergence of iterative algorithms [31]. At the t th iteration, the message is damped by obtaining a convex combination of the message computed at the t th iteration and the message at the $(t-1)$ th iteration, with a damping factor $\Delta \in [0, 1]$. Thus, if \tilde{p}_i^t is the computed probability at the t th iteration, the message at the end of t th iteration is

$$p_i^t = (1 - \Delta)\tilde{p}_i^t + \Delta p_i^{t-1}. \quad (19)$$

In section III-D, we will see the performance of these methods in improving the rate of convergence and the optimal choice for Δ .

A listing of the proposed MPD algorithm with damping is given in **Algorithm 1**, where $\mathbf{p} = [p_1 \ p_2 \ \dots \ p_{2K}]^T$ and $\tilde{\mathbf{p}} = [\tilde{p}_1 \ \tilde{p}_2 \ \dots \ \tilde{p}_{2K}]^T$.

C. Complexity comparison between MPD and MMSE

The computational complexity of the MPD algorithm is as follows. The complexity (in number of real operations) required to compute (11), (12) and (16) is of order $O(K^2)$. The complexities of computing \mathbf{z} and \mathbf{J} are of orders $O(NK)$ and $O(\bar{N}K^2)$, respectively. So, the total complexity of the proposed MPD is $O(NK^2)$, which is attractive for large-scale MIMO systems.

In Table I, we present an interesting comparison between the complexities of MPD and MMSE detection for $N = 128, 256$, and K varied from 16 to 256 . Since we have used 20 iterations for MPD in all the BER simulations, we have taken the number of iterations to be 20 for the calculation of the MPD complexity. From Table I, the following interesting observations can be made: 1) for large N (e.g., $N = 256$), MPD complexity is less than MMSE complexity. This is because MPD needs only matrix multiplication and not matrix inversion, whereas MMSE detection needs both matrix multiplication and inversion; 2) for $N = 128$, the MPD complexity for $K = 64, 96, 128$ is less than the MMSE complexity. For $K = 16, 32$, the MPD complexity is almost

| K | Complexity in number of real operations $\times 10^6$ | | | | | |
|-----|---|------------|---------------|---------|------------|---------------|
| | N = 128 | | | N = 256 | | |
| | MMSE | MPD (prop) | SUMIS in [37] | MMSE | MPD (prop) | SUMIS in [37] |
| 16 | 0.177 | 0.179 | 0.483 | 0.333 | 0.296 | 0.917 |
| 32 | 0.748 | 0.749 | 1.737 | 1.321 | 1.190 | 3.130 |
| 64 | 3.593 | 3.200 | 7.538 | 5.789 | 4.773 | 12.420 |
| 96 | 9.584 | 7.208 | 19.368 | 14.450 | 10.748 | 29.837 |
| 128 | 19.770 | 12.814 | 39.194 | 28.355 | 19.116 | 57.347 |
| 256 | - | - | - | 157.373 | 76.505 | 307.633 |

TABLE I
COMPARISON BETWEEN THE COMPLEXITIES (IN NUMBER OF REAL OPERATIONS) OF THE PROPOSED MPD, MMSE DETECTOR, AND SUMIS DETECTOR IN [37] FOR DIFFERENT VALUES OF K, N . NUMBER OF ITERATIONS FOR MPD = 20, AND $n_s = 3$ FOR SUMIS.

the same as (marginally higher than) MMSE complexity, because the number of iterations ($= 20$) is comparable with K ($= 16, 32$). Also, MPD performs better than MMSE detection, and achieves close to optimal detection performance for large K, N , and different system loading factors. We will see this performance advantage of MPD in the following subsection.

D. BER performance of MPD

In this subsection, we present the uncoded BER performance of MPD obtained through simulations for different system parameter settings. We will now assume perfect knowledge \mathbf{H} . We will relax this assumption later. First, in Fig. 4, we plot the uncoded BER of MPD at an average SNR of 12 dB for $N = K = 64$ for various values of the damping factor Δ . The number of message passing iterations used is 20. From this figure, we observe that a damping factor of $\Delta = 0.33$ is optimal. This value of Δ is found to give good performance for other values of system parameters as well. So we have used this value of Δ in all the simulations. Next, Fig. 5 shows the uncoded BER of MPD as a function of iteration index with and without Aitken acceleration for $N = K = 64$, SNR=12 dB, and $\Delta = 0.33$. It can be observed that the convergence rate of the algorithm improves with Aitken acceleration.

In Fig. 6, we plot the uncoded BER of MPD for different values of N ($= 4, 8, 16, 32, 64, 128$) for a system loading factor of $\alpha = 1$ ($K = N$). Since optimal detection performance for large-dimension systems is hard to obtain, we have plotted single-input single-output (SISO) additive white Gaussian noise (AWGN) channel performance as a lower bound on the optimum detection performance. MMSE detection performance is also plotted for comparison. From Fig. 6, it is observed that the performance of MPD improves for increasing N, K , and moves closer to the SISO-AWGN performance for large N, K . For example, the MPD performance for $N = K = 128$ gets very close to SISO-AWGN performance. It is also observed that MPD performance is better than MMSE detection performance.

Figure 7 shows the uncoded BER of MPD algorithm and

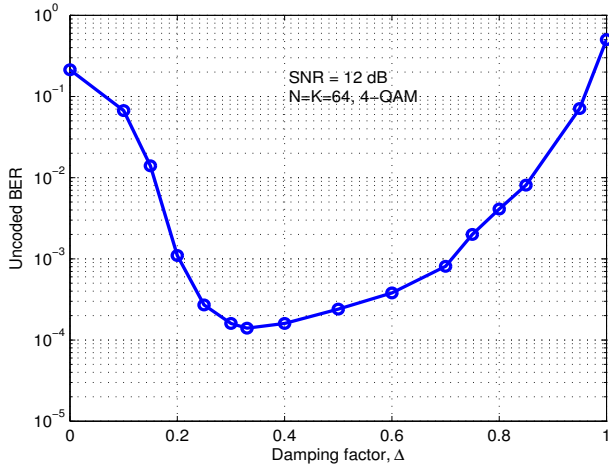


Fig. 4. Uncoded BER performance of the proposed MPD algorithm as a function of damping factor Δ . $N = K = 64$, 4-QAM, $\text{SNR}=12 \text{ dB}$.

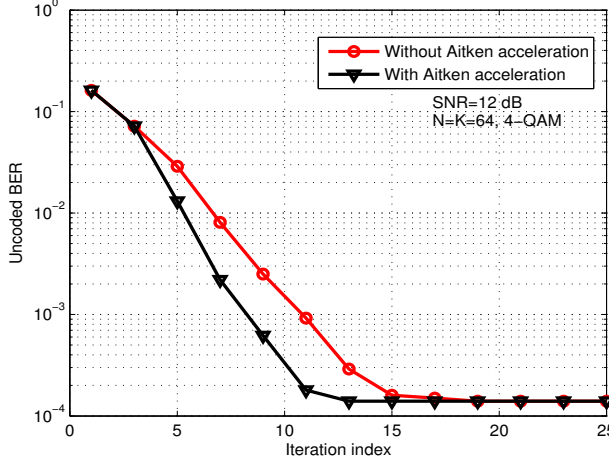


Fig. 5. Comparison of the convergence behavior of the MPD algorithm without and with Aitken acceleration. $N = K = 64$, 4-QAM, $\text{SNR}=12 \text{ dB}$.

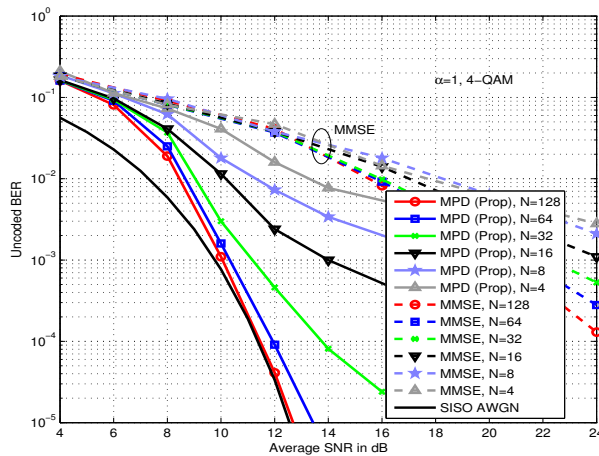


Fig. 6. Uncoded BER performance of the MPD algorithm and the MMSE detector for $N = K = 4, 8, 16, 32, 64, 128$, 4-QAM.

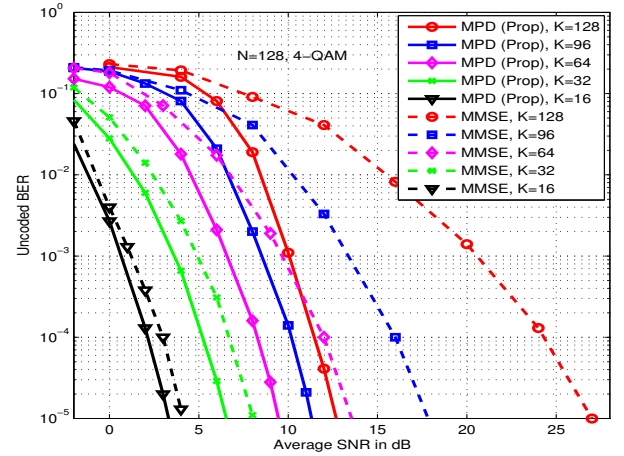


Fig. 7. Uncoded BER performance of the MPD algorithm and the MMSE detector for different values of K ($= 16, 32, 64, 96, 128$) for a fixed $N = 128$, 4-QAM.

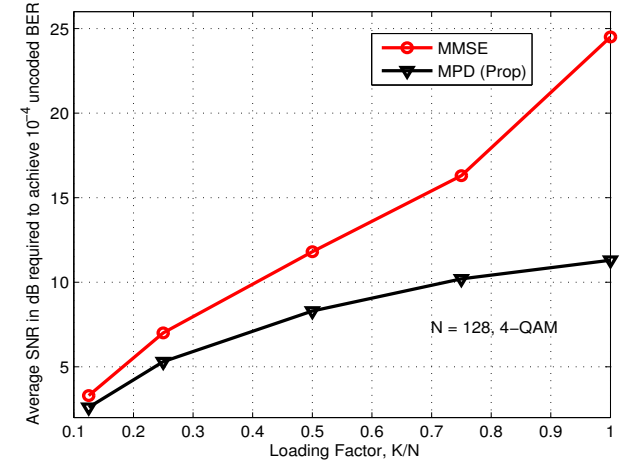


Fig. 8. Comparison between the average SNR required to achieve an uncoded BER of 10^{-4} in MPD and MMSE detection at different loading factors with $N = 128$, 4-QAM.

MMSE detector for a fixed number of receiver antennas at the BS ($N = 128$) and varying number of users ($K = 16, 32, 64, 96, 128$), i.e., for different values of loading factors ($\alpha = \frac{1}{8}, \frac{1}{4}, \frac{1}{2}, \frac{3}{4}, 1$). It is observed that the BER performance improves considerably as the loading factor is reduced, which is expected. The MPD performance for different loading factors is better than MMSE detection performance. This observation is further illustrated in Fig. 8, where the average SNRs required to achieve an uncoded BER of 10^{-4} in MPD and MMSE detection are plotted. It can be observed from Fig. 8 that the MPD outperforms the MMSE detection by about 1.2 dB at a loading factor of $\alpha = 0.125$. This performance advantage of MPD over MMSE detection increases for increasing values of α . For example, the performance advantage of MPD over MMSE detection is about 6.5 dB and 12.5 dB for $\alpha = 0.75$ and $\alpha = 1$, respectively. The reason why MMSE

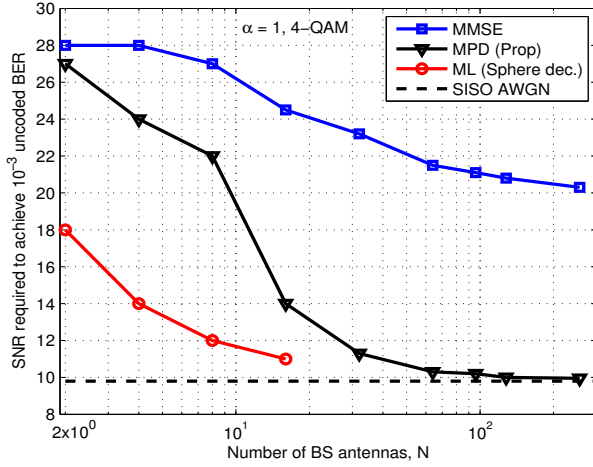


Fig. 9. Comparison between the average SNR required to achieve an uncoded BER of 10^{-3} BER in ML (sphere decoding), MPD, and MMSE detection as a function of N for $\alpha = 1$ (i.e., $N = K$) and 4-QAM.

detection performs quite poorly at high loading factors is because the spatial interference gets increased significantly at higher loading factors with large N (e.g., $N = K = 128$) compared to lower loading factors, and MMSE detection does not perform interference cancellation/suppression. Whereas, the MPD is benefited by the channel hardening effect with large N, K . The performance advantage of MPD becomes very attractive given that MPD complexity is almost same or less than the MMSE detection complexity (as discussed in Section III-C).

The effect of channel hardening on the BER performance of the MPD algorithm is further illustrated in Fig. 9. This figure shows the SNRs required to achieve 10^{-3} BER with MPD as well as MMSE detection in $N = K = 2$ to $N = K = 256$ systems. We have also plotted the same for ML detection (using sphere decoding) in $N = K = 2$ to $N = K = 16$ systems. Since ML detection is prohibitive for larger dimensions, we have plotted the SNR required in a SISO AWGN system as a lower bound on the ML performance. In small systems like $N = K = 2, 4, 8$ systems where channel hardening is not significant, both MPD and MMSE performances are far from ML performance with MPD performing better than MMSE – e.g., MPD performance is about 10 dB away from ML performance in $N = K = 4, 8$ systems, whereas MMSE performance is about 14 to 15 dB away from ML performance in $N = K = 4, 8$ systems. In systems with size larger than $N = K = 16$, channel hardening becomes more significant and the performance of MPD shows significant improvement compared to MMSE and gets closer to ML performance – e.g., for $N = K = 128$ system, the MPD performance is just about 0.25 dB away from the ML lower bound whereas the MMSE performance is away from the ML lower bound by about 10 dB. These observations illustrate that harder the channel gets, better is the MPD performance.

E. Channel estimation for MPD

A key issue in large-scale MIMO systems is the estimation of channel gains. In conventional approaches, the NK channel gains in the channel matrix are estimated and used for the detection of transmitted symbols. Note that in our transformed system model (7), the influence of the channel on vector \mathbf{z} is through $\mathbf{H}^T \mathbf{H}$, rather than through \mathbf{H} as such. We propose to exploit this observation on the structure of the system model (7). Specifically, we propose to directly obtain an estimate of $\mathbf{H}^T \mathbf{H}$ and use it in the MPD algorithm, rather than obtaining an estimate of \mathbf{H} as done in conventional approaches. We note that this approach is simple and novel, and it works very well in the MPD algorithm (as we will see in the performance results). We present the scheme to obtain an estimate of the $\mathbf{H}^T \mathbf{H}$ matrix next.

Estimating the $\mathbf{H}^T \mathbf{H}$ matrix:

Note that we have defined $\mathbf{J} = \mathbf{H}^T \mathbf{H}$. We are interested in obtaining $\hat{\mathbf{J}}$, an estimate of \mathbf{J} . We assume that the channel is slowly fading, where the channel matrix \mathbf{H} remains constant over one frame duration (which is taken to be equal to the coherence time of the channel). The length of one frame is L_f channel uses. Each frame consists of a pilot part and a data part. The pilot part consists of K channel uses, and the data part consists of $L_f - K$ channel uses.

Let $\mathbf{X}_p = PI_K$ denote the pilot matrix, where in the i th channel use, $1 \leq i \leq K$, user i transmits a pilot tone with amplitude P and the other users remain silent. The received pilot matrix at the BS is then given by

$$\begin{aligned} \mathbf{Y}_p &= \mathbf{H} \mathbf{X}_p + \mathbf{W}_p \\ &= \mathbf{P} \mathbf{H} + \mathbf{W}_p, \end{aligned} \quad (20)$$

where $P = \sqrt{KE_s}$, E_s is the average symbol energy, and \mathbf{W}_p is the noise matrix. Using Lemma 1, we obtain an estimate of the matrix \mathbf{J} as

$$\hat{\mathbf{J}} = \frac{\mathbf{Y}_p^T \mathbf{Y}_p}{NP^2} - \frac{\sigma_v^2}{P^2} \mathbf{I}_K. \quad (21)$$

An estimate of the vector \mathbf{z} is obtained as

$$\hat{\mathbf{z}} = \frac{\mathbf{Y}_p^T \mathbf{y}}{NP}. \quad (22)$$

The estimates $\hat{\mathbf{J}}$ and $\hat{\mathbf{z}}$ are used as inputs to the MPD algorithm in place of \mathbf{J} and \mathbf{z} .

Note on complexity:

A key advantage of the above estimation scheme is its low complexity. The computation of $\hat{\mathbf{J}}$ and $\hat{\mathbf{z}}$ in (21) and (22) requires only matrix and vector multiplications. Note that even when perfect knowledge of \mathbf{H} or an estimate of \mathbf{H} is available, similar computations are needed to compute \mathbf{J} and \mathbf{z} . Further note that the additional complexity needed to obtain an estimate of \mathbf{H} in the conventional approach is avoided in our approach.

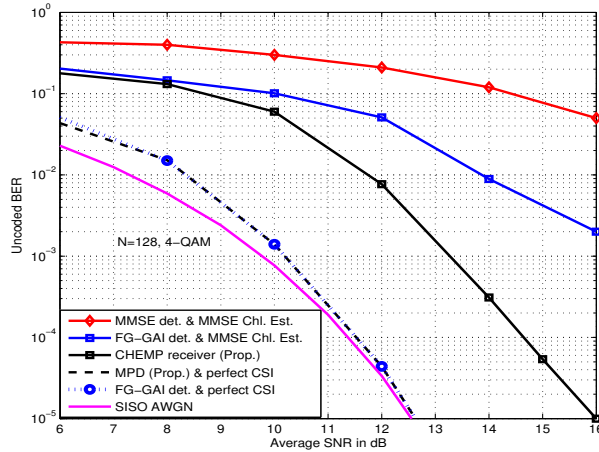


Fig. 10. Comparison of the BER performance of the proposed CHEMP receiver with those of 1) MMSE detector with MMSE channel estimate, and 2) FG-GAI detector in [11] with MMSE channel estimate, for $N = K = 128$, 4-QAM.

F. BER performance of the CHEMP receiver

As mentioned before, we refer to the combination of proposed MPD algorithm and the channel estimation scheme proposed in the previous subsection as the CHEMP receiver. In this subsection, we present the uncoded BER performance of the CHEMP receiver. The number of iterations used in the MPD algorithm is 20. We compare the performance of the CHEMP receiver with two other receivers, namely, 1) MMSE detector with MMSE channel estimate, and 2) FG-GAI (factor graph with Gaussian approximation of interference) detector in [11] with MMSE channel estimate. We note that the FG-GAI detector in [11] is also a message passing algorithm which used a Gaussian approximation of interference. But this approximation was done on the original system model in (2), whereas in the proposed MPD algorithm, the Gaussian approximation is done on the matched filtered system model in (7).

In Fig. 10, we present an uncoded BER performance comparison between 1) proposed CHEMP receiver, 2) MMSE detector with MMSE channel estimate, and 3) FG-GAI detector in [11] with MMSE channel estimate. It can be seen that the performance of the proposed CHEMP receiver is significantly better than those of the MMSE and FG-GAI detectors with MMSE estimate of the channel. Observe that the performances of MPD and FG-GAI under perfect CSI conditions are almost the same, whereas under estimated CSI conditions, the CHEMP receiver performs significantly better than FG-GAI with MMSE channel estimate. An analytical reasoning for this is presented in Section IV-B.

Figure 11 shows the performance of the CHEMP receiver and MMSE detector with MMSE channel estimate for different number of users ($K = 16, 32, 64, 96, 128$) and fixed number of BS antennas ($N = 128$). As expected, the performance

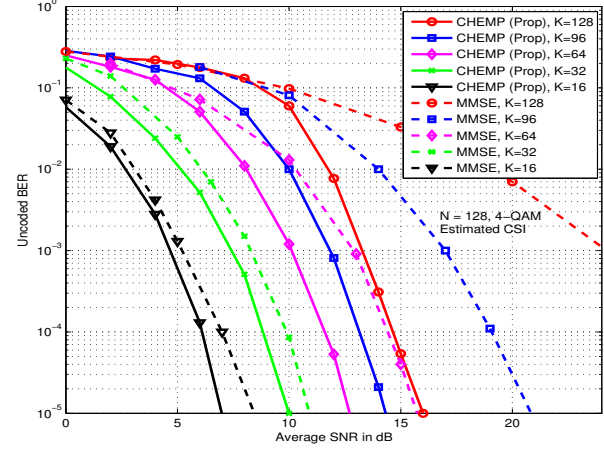


Fig. 11. BER performance of 1) proposed CHEMP receiver and 2) MMSE detector with MMSE channel estimate, for different values of K ($= 16, 32, 64, 96, 128$) for a fixed value of N ($= 128$), 4-QAM.

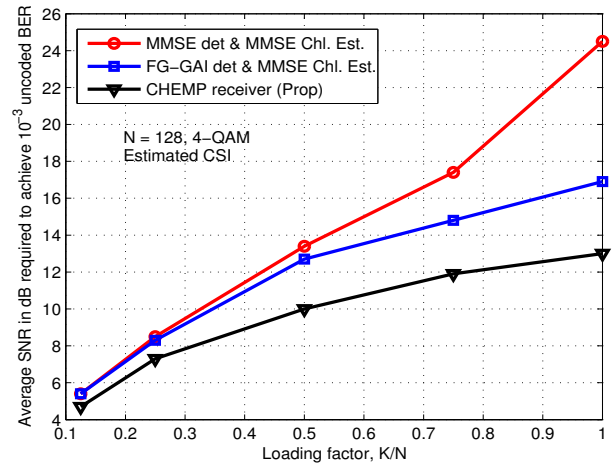


Fig. 12. Comparison between the average SNR required to achieve an uncoded BER of 10^{-3} in 1) proposed CHEMP receiver, 2) MMSE detector with MMSE channel estimate, and 3) FG-GAI detector in [11] with MMSE channel estimate, at different loading factors with $N = 128$, 4-QAM.

improves for smaller values of K . Also, CHEMP receiver performs better than MMSE detector with MMSE channel estimate. In Fig. 12, we illustrate a comparison between the the average SNR required to achieve an uncoded BER of 10^{-3} in 1) proposed CHEMP receiver, 2) MMSE detector with MMSE channel estimate, and 3) FG-GAI detector in [11] with MMSE channel estimate, at different loading factors with $N = 128$. From this figure, we observe that the CHEMP receiver outperforms the other two receivers. For example, the CHEMP receiver outperforms the MMSE detector with MMSE channel estimate by about 0.6 dB to 11 dB for loading factors in the range of $\alpha = 0.125$ to $\alpha = 1$. Likewise, the performance advantage of the CHEMP receiver over FG-GAI detector with MMSE channel estimate is about 0.6 dB to 4 dB for loading factors in the range of $\alpha = 0.125$ to $\alpha = 1$.

G. Comparison with SUMIS detector in [37]

A subspace marginalization with interference suppression (SUMIS) detector has been proposed recently in [37]. The SUMIS detector uses the ideas of partial marginalization (via a parameter $n_s \in \{1, 2, \dots, K\}$) and soft interference suppression. The order of complexity of the SUMIS detector is $K^3 + 2NK + K^2(2n_s^2 + 6)$ [37]. Here, we present a performance and complexity comparison between the proposed MPD and the SUMIS detector. Figure 13 shows the BER performance of the proposed MPD and SUMIS detector (with $n_s = 3$) for various values of K keeping N fixed at 128, 4-QAM, and perfect CSI. For the same system parameters, Fig. 14 shows the comparison between the proposed CHEMP receiver and SUMIS detector with MMSE channel estimate. These figures show that the proposed MPD/CHEMP performs better than SUMIS with MMSE channel estimate. The proposed detector achieves better performance at less complexity than SUMIS detector. This can be observed in Table I which presents the complexities of MPD and SUMIS for different values of N and K . The complexity advantage of the proposed MPD over SUMIS is because MPD needs only matrix multiplication and not matrix inversion, whereas SUMIS needs both matrix multiplication and matrix inversion.

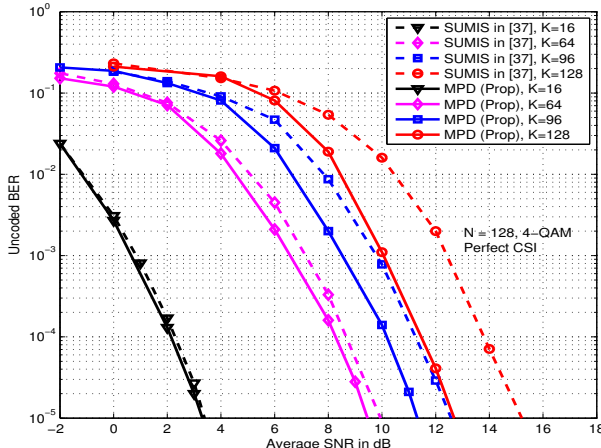


Fig. 13. BER performance of 1) proposed MPD detector and 2) SUMIS detector in [37] for different values of K ($= 16, 64, 96, 128$) for a fixed value of N ($= 128$), 4-QAM, perfect CSI.

IV. ANALYSIS OF THE PROPOSED CHEMP RECEIVER

In this section, we carry out some analysis of the proposed CHEMP receiver. The analysis reported in this section has two parts. In the first part, we analyze the convergence of the proposed MPD algorithm, and give a sufficient condition for the algorithm to converge to the correct solution. In the second part, we present an analysis of the mean square difference (MSD) of the LLRs computed with estimated CSI and perfect CSI for the proposed CHEMP receiver as well

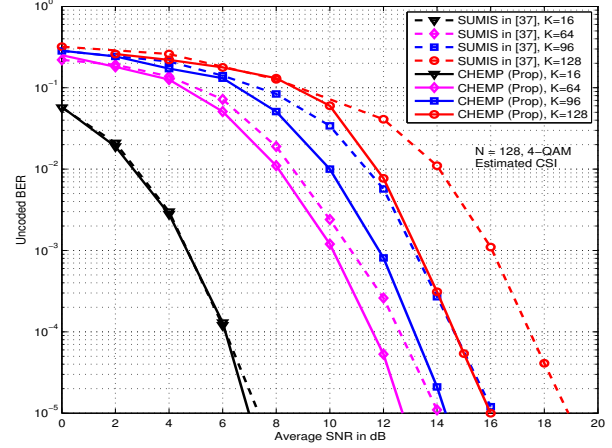


Fig. 14. BER performance of 1) proposed CHEMP receiver and 2) SUMIS detector with MMSE channel estimate for different values of K ($= 16, 32, 64, 128$) for a fixed value of N ($= 128$), 4-QAM.

as the FG-GAI receiver (i.e., FG-GAI detector in [11] with MMSE channel estimate).

A. Analysis of the convergence of MPD algorithm

First we state the lemmas that we require to prove results in the later parts of this subsection. Let \mathcal{P} denote the set $\{\mathbf{p} \mid \mathbf{p} \in [0, 1]^{2K}\}$.

Lemma 2. *The set \mathcal{P} is a compact and convex set.*

Proof: Since every element p_i of any $\mathbf{p} \in \mathcal{P}$ is from the same closed compact interval $[0, 1] \subset \mathbb{R}$, \mathcal{P} is also a closed subset of \mathbb{R}^{2K} , and hence \mathcal{P} is also a compact subset. Let \mathbf{p}_1 and \mathbf{p}_2 be any two elements of \mathcal{P} . Then it can be seen that for any $\lambda \in [0, 1]$,

$$\lambda \mathbf{p}_1 + (1 - \lambda) \mathbf{p}_2 \in \mathcal{P}. \quad (23)$$

Hence, \mathcal{P} is a convex set. This set \mathcal{P} is the compact convex subset of \mathbb{R}^{2K} consisting of all probability vectors. \blacksquare

We define the following variables for convenience:

$$\begin{aligned} V_i^+(\mathbf{p}) &\triangleq z_i - J_{ii} - \sum_{j=1, j \neq i}^{2K} J_{ij}(2p_j - 1), \\ V_i^-(\mathbf{p}) &\triangleq z_i + J_{ii} - \sum_{j=1, j \neq i}^{2K} J_{ij}(2p_j - 1), \end{aligned} \quad (24)$$

$$\begin{aligned} A_i^+(\mathbf{p}) &\triangleq \frac{-1}{2\sigma_i^2} (V_i^+(\mathbf{p}))^2, & A_i^-(\mathbf{p}) &\triangleq \frac{-1}{2\sigma_i^2} (V_i^-(\mathbf{p}))^2, \\ f_i^+(\mathbf{p}) &\triangleq \exp(A_i^+(\mathbf{p})), & f_i^-(\mathbf{p}) &\triangleq \exp(A_i^-(\mathbf{p})), \end{aligned} \quad (25)$$

where z_i, J_{ij}, σ_i are constants in \mathbb{R} , $\sigma_i > 0$ and $\mathbf{p} \in \mathcal{P}$.

Lemma 3. *Let $f(\mathbf{p})$ be a function such that if $\mathbf{p}' = f(\mathbf{p})$ then $p'_i = f_i(\mathbf{p}) \triangleq \frac{f_i^+(\mathbf{p})}{f_i^+(\mathbf{p}) + f_i^-(\mathbf{p})}$. Then $f(\mathbf{p})$ is continuous in \mathcal{P} .*

Proof: We see that $f : \mathcal{P} \rightarrow \mathcal{P}$. Since $A_i^+(\mathbf{p})$ and $A_i^-(\mathbf{p})$ are polynomial functions in $p_j, j \in \{1, \dots, 2K\} \setminus i$ and $\exp(\cdot)$ is a continuous monotone function, $f_i^+(\mathbf{p})$ and $f_i^-(\mathbf{p})$ are continuous functions in \mathcal{P} . Since \mathbf{p} belongs to a closed set and $\exp(\cdot)$ is a non-negative function, the term $(f_i^+(\mathbf{p}) + f_i^-(\mathbf{p}))$ is always positive. Hence, $f_i(\mathbf{p})$ being a ratio of two continuous functions with non-vanishing denominator, is also a continuous function. This proves that $f(\mathbf{p})$ is continuous in \mathcal{P} , as all its component functions are continuous in \mathcal{P} . \blacksquare

From Lemma 3 we see that $f(\mathbf{p})$ is a recursive map that represents the proposed MPD algorithm in Section III-A.

Proposition 1. *The function $f(\mathbf{p})$ defined in Lemma 3 has a fixed point in \mathcal{P} .*

Proof: By Lemma 2, \mathcal{P} is a compact convex set and by Lemma 3, $f(\mathbf{p})$ is a continuous function such that $f : \mathcal{P} \rightarrow \mathcal{P}$. Hence, by Brouwer's fixed point theorem [36], $f(\mathbf{p})$ has a fixed point in \mathcal{P} . \blacksquare

Proposition 1 proves that the proposed MPD algorithm has a fixed point.

Now, we give a sufficient condition for the MPD algorithm to converge to the correct solution. Since the Gaussian distribution is a symmetric function with its positive part being monotone decreasing, we have $p'_i > \frac{1}{2}$ in the function $\mathbf{p}' = f(\mathbf{p})$ whenever $V_i^+(\mathbf{p})^2 < V_i^-(\mathbf{p})^2$. Let

$$\begin{aligned} d_i &\triangleq V_i^+(\mathbf{p})^2 - V_i^-(\mathbf{p})^2 \\ &= -4J_{ii} \left[J_{ii}x_i + \sum_{j=1, j \neq i}^{2K} J_{ij}(x_j - 2p_j + 1) + n_i \right]. \end{aligned} \quad (26)$$

We know that $J_{ii} > 0, \forall i$. When $x_i = +1, p'_i > \frac{1}{2}$ iff $d_i < 0$, and d_i will be negative irrespective of \mathbf{p} iff

$$J_{ii} + \sum_{j=1, j \neq i}^{2K} J_{ij}(x_j - 2p_j + 1) + n_i > 0. \quad (27)$$

Bounding the $J_{ij}(x_j - 2p_j + 1)$ term on the LHS of (27) by $-2|J_{ij}|$, at high SNRs, we get

$$J_{ii} > 2 \sum_{j=1, j \neq i}^{2K} |J_{ij}|. \quad (28)$$

It can be similarly shown that (28) should be true for $d_i > 0$ when $x_i = -1$, irrespective of \mathbf{p} . Thus, when (28) is true the MPD algorithm has a fixed point that is provably unique and attractive.

When the algorithm starts with an initial vector of $p_i = 0.5, \forall i$, then the condition in (28) can be simplified to

$$J_{ii} > \sum_{j=1, j \neq i}^{2K} |J_{ij}|, \quad (29)$$

which is nothing but the diagonal dominance condition for the matrix \mathbf{J} , and it gives a sufficient condition for the MPD

algorithm to converge to the correct solution. It should be noted that (29) is not a necessary condition for convergence. From extensive simulations, it has been observed that the MPD algorithm performs very well for large N, K even when the matrix \mathbf{J} is not diagonally dominant.

B. Analysis of LLRs in CHEMP and FG-GAI receivers

In Fig. 10, we observed that while the performances of MPD and FG-GAI under perfect CSI conditions are almost the same, under estimated CSI conditions, the CHEMP receiver performs significantly better than FG-GAI with MMSE channel estimate. Here, we shall present an LLR analysis that explains the reason for this performance advantage of CHEMP receiver under estimated CSI conditions.

We note that there are three different LLRs of interest here, which we call as Type-1 LLR, Type-2 LLR, and Type-3 LLR. Type-1 LLR is the 'true' LLR in the 'exact' MAP detector. Type-2 LLR is an approximate LLR in a detector (e.g., MPD, FG-GAI detectors) with perfect CSI. Type-3 LLR is an approximate LLR in a detector with estimated CSI. A comparison between the Type-1 LLR and Type-2 LLR of MPD for large dimensions like $N = K = 128$ is infeasible because of the exponential complexity of the computation of LLRs in the exact MAP detector. For the purpose of analytically reasoning the performance advantage of the CHEMP receiver, we use a performance measure which is the mean square difference (MSD) between 1) Type-2 and Type-3 LLRs of the MPD detector, and 2) Type-2 and Type-3 LLRs of the FG-GAI detector. This MSD measure for a given detector can be viewed as an indicator of the relative degradation of the LLR of the detector computed under perfect CSI to that computed under estimated CSI. In the following, we derive upper bounds on the MSD of LLRs in CHEMP receiver and FG-GAI with MMSE channel estimate.

The signal vector $\hat{\mathbf{z}}$ in the CHEMP receiver given by (22) can be written as

$$\begin{aligned} \hat{\mathbf{z}} &= \frac{1}{NP} (\mathbf{Y}_p^T \mathbf{H} \mathbf{x} + \mathbf{Y}_p^T \mathbf{w}) \\ &= \underbrace{\left(\mathbf{J} + \frac{\mathbf{W}_p^T \mathbf{H}}{NP} \right) \mathbf{x}}_{\triangleq \tilde{\mathbf{J}}} + \underbrace{\left(\frac{\mathbf{H}}{N} + \frac{\mathbf{W}_p}{NP} \right)^T \mathbf{w}}_{\triangleq \tilde{\mathbf{w}}} \\ &= \tilde{\mathbf{J}} \mathbf{x} + \tilde{\mathbf{w}}. \end{aligned} \quad (30)$$

Likewise, the matrix $\hat{\mathbf{J}}$ in the CHEMP receiver given by (21) can be written as

$$\begin{aligned} \hat{\mathbf{J}} &\triangleq \frac{(\mathbf{P}\mathbf{H} + \mathbf{W}_p)^T (\mathbf{P}\mathbf{H} + \mathbf{W}_p)}{NP^2} - \frac{\sigma_v^2}{P^2} \mathbf{I}_K \\ &= \left(\mathbf{J} + \frac{\mathbf{W}_p^T \mathbf{H}}{NP} \right) + \underbrace{\frac{1}{NP} \left(\mathbf{H}^T \mathbf{W}_p + \frac{\mathbf{W}_p^T \mathbf{W}_p}{P} \right)}_{\triangleq \tilde{\mathbf{J}}'} - \frac{\sigma_v^2}{P^2} \mathbf{I}_K \\ &= \tilde{\mathbf{J}} + \tilde{\mathbf{J}}'. \end{aligned} \quad (31)$$

Note that, as per (30), the detection of \mathbf{x} requires an estimate of $\tilde{\mathbf{J}}$. But the CHEMP receiver uses $\hat{\mathbf{J}}$ instead. This, as per (31), amounts to using an estimate of $\tilde{\mathbf{J}}$ with an estimation error of $\tilde{\mathbf{J}}'$.

Assume N and K are large and all the transmitted bits are i.i.d. Let δ prefixed to a variable denote the difference between the variable computed under estimated CSI (i.e., using $\hat{\mathbf{J}}$ and $\hat{\mathbf{z}}$) and perfect CSI (i.e., using \mathbf{J} and \mathbf{z}). For example, $\delta\mu_i = \hat{\mu}_i - \mu_i$, where $\hat{\mu}_i$ is obtained by substituting $\hat{\mathbf{J}}$ in place of \mathbf{J} in (11). Likewise, $\delta L_i = \hat{L}_i - L_i$, where \hat{L}_i obtained by substituting $\hat{\mathbf{J}}$ and $\hat{\mathbf{z}}$ in place of \mathbf{J} and \mathbf{z} , respectively, in (15).

Now, from (15), we can write the LLR computed by the CHEMP receiver as

$$\hat{L}_i = \frac{2\tilde{J}_{ii} + 2\tilde{J}'_{ii}}{\sigma_i^2 + \delta\sigma_i^2}(\hat{z}_i - \mu_i - \delta\mu_i). \quad (32)$$

Now, δL_i is bounded above as

$$\delta L_i \leq \frac{2\tilde{J}'_{ii}(\hat{z}_i - \mu_i - \delta\mu_i) - 2\tilde{J}_{ii}\delta\mu_i}{\sigma_i^2}. \quad (33)$$

By Lemma 1, we can write the following:

$$\tilde{J}'_{ij|i \neq j} \sim \mathcal{N}\left(0, \frac{\sigma_v^4}{NP^4} + \frac{\sigma_v^2}{2NP^2}\right), \quad (34)$$

$$\tilde{J}'_{ii} \sim \mathcal{N}\left(0, \frac{2\sigma_v^4}{NP^4} + \frac{\sigma_v^2}{2NP^2}\right), \quad (35)$$

$$\delta\mu_i \sim \mathcal{N}\left(0, \frac{\sigma_v^4}{P^4} + \frac{\sigma_v^2}{2P^2}\right). \quad (36)$$

Without loss of generality, we can assume $P = 1$. Therefore, $\mathbb{E}(\delta L_i) = 0$, and

$$\mathbb{E}(\delta L_i^2) \leq \frac{\sigma_e^2}{\sigma_i^4} \left\{ \alpha \left(\sigma_v^2 + \frac{1}{2} \right) + \left(\alpha(\sigma_v^4 + \frac{\sigma_v^2}{2}) + (z_i - \mu_i)^2 \right) \cdot \left(\frac{8\sigma_v^2}{N} + \frac{2}{N} \right) \right\}. \quad (37)$$

Note that $\mathbb{E}(\delta L_i^2)$ is the MSD between the Type-2 and Type-3 LLRs of the MPD.

Next, we do a similar analysis of the MSD of LLRs for the FG-GAI detector. Using the definition of the LLRs Λ_i^k in the FG-GAI detector as given in [11], the difference in LLR in FG-GAI computed with MMSE channel estimate and that computed with perfect CSI is bounded above as

$$\delta\Lambda_i^k \leq \frac{4H'_{ik}(y_i - \mu_{ik} - \delta\mu_{ik}) - 4H_{ik}\delta\mu_{ik}}{\sigma_{ik}^2}, \quad (38)$$

where the terms μ_{ik} and σ_{ik}^2 are as defined in [11], H'_{ij} is the error in estimating H_{ij} , and, as defined before, δ prefixed to a variable denotes the difference between that variable computed under estimated CSI and perfect CSI. The error in the MMSE channel estimate in the FG-GAI receiver is

$$H'_{ij} = \frac{W_{ij}P - H_{ij}\sigma_n^2}{P^2 + \sigma_n^2}, \quad (39)$$

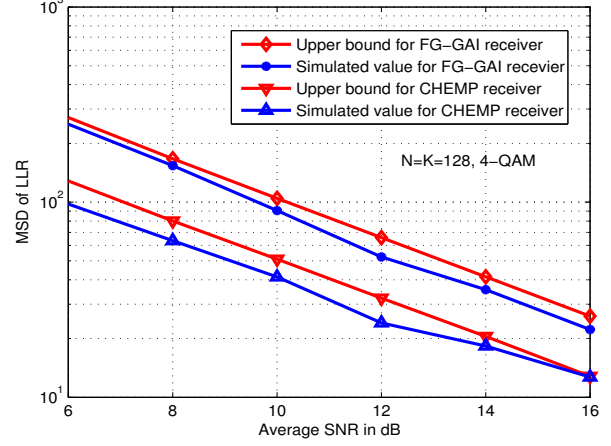


Fig. 15. MSD of LLRs in FG-GAI and CHEMP receivers for $N = K = 128$, 4-QAM.

where W_{ij} is the (i, j) th element in matrix \mathbf{W}_P . The statistics of H'_{ij} are computed by using Lemma 1 as follows:

$$\mathbb{E}(H'_{ij}) = 0, \quad \sigma_e^2 \triangleq \mathbb{E}(H'_{ij}^2) = \frac{\sigma_n^2(P^2 + \frac{\sigma_n^2}{2})}{(P^2 + \sigma_n^2)^2}. \quad (40)$$

Without loss of generality, assume $P = 1$ and $\alpha = 1$. Now, we have $H'_{ij} \sim \mathcal{N}(0, \sigma_e^2)$ and $\delta\mu_{ij} \sim \mathcal{N}(0, N\sigma_e^2)$. By Lemma 1, we have $\mathbb{E}(\delta\Lambda_i^j = 0)$, and

$$\mathbb{E}((\delta\Lambda_i^j)^2) \leq \frac{16\sigma_e^2}{\sigma_{ij}^4} \left(N \left(\sigma_e^2 + \frac{1}{2} \right) + (y_i - \mu_{ij})^2 \right). \quad (41)$$

The probability of the i th symbol is computed using the LLR value $L_i^F \triangleq \sum_{l \neq i}^N \Lambda_l^j$. Therefore, $\delta L_i^F = \sum_{l \neq i}^N \delta\Lambda_l^j$, $\mathbb{E}(\delta L_i^F) = 0$, and $\mathbb{E}((\delta L_i^F)^2) = (N-1)\mathbb{E}(\delta\Lambda_i^j)^2$. It is noted that $\mathbb{E}((\delta L_i^F)^2)$ is the MSD between the Type-2 and Type-3 LLRs of the FG-GAI detector.

It can be seen from (37) and (41) that the MSD of the computed LLR values in each iteration is less in the CHEMP receiver compared to that in the FG-GAI receiver. This is further verified by simulation in Fig. 15, where it can be observed that the simulated MSD of the LLRs in the CHEMP receiver is less compared to that in the FG-GAI receiver. This makes the proposed CHEMP receiver robust to channel estimation errors when compared to the FG-GAI receiver.

V. EXTENSION TO HIGHER-ORDER QAM

In this section, we extend the MPD algorithm to higher-order QAM. For M -QAM alphabets, the elements of \mathbf{x} in (2) belong to the underlying PAM alphabet; for example, when the transmitted symbols are from 16-QAM alphabet, the elements of \mathbf{x} are 4-PAM symbols. In such a scenario, we compute symbol-wise probability messages in the MPD algorithm. Specifically, in each iteration, for each element in \mathbf{x} , we compute the probability masses for all symbols in \mathbb{B}

as follows. The means are computed as

$$\begin{aligned}\mu_i &= \sum_{j=1, j \neq i}^{2K} J_{ij} \mathbb{E}(x_j) \\ &= \sum_{j=1, j \neq i}^{2K} J_{ij} \sum_{s \in \mathbb{B}} s p_j(s).\end{aligned}\quad (42)$$

The variances are computed as

$$\begin{aligned}\sigma_i^2 &= \sum_{j=1, j \neq i}^{2K} J_{ij}^2 \text{Var}(x_j) + \sigma_v^2 \\ &= \sum_{j=1, j \neq i}^{2K} J_{ij}^2 \left(\sum_{s \in \mathbb{B}} s^2 p_j(s) - \mathbb{E}(x_j)^2 \right) + \sigma_v^2,\end{aligned}\quad (43)$$

where σ_v^2 is as defined in Section III-A. The probability of x_i being $s \in \mathbb{B}$ is computed as

$$p_i(s) \propto \exp \left(\frac{-1}{2\sigma_i^2} (z_i - \mu_i - J_{ii}s)^2 \right). \quad (44)$$

Finally, the bit probabilities are obtained as

$$\Pr(b_i^p = 1) = \sum_{\substack{s \in \mathbb{B}: \\ \text{pth bit in } s \text{ is } 1}} p_i(s), \quad (45)$$

where b_i^p is the p th bit in the i th user's symbol, which is detected as 1 if $\Pr(b_i^p = 1) \geq 0.5$ and 0 otherwise. It can be noted that the message passed by each node is a vector of length $|\mathbb{B}|$.

Complexity: The complexity of computation of \mathbf{z} and \mathbf{J} are $O(NK)$ and $O(NK^2)$, respectively. The complexity of computing the messages is $O(\sqrt{MK^2})$ for a square M -QAM constellation. This is due to the vector nature of the messages for M -QAM alphabet as opposed to the scalar messages for $\{\pm 1\}$ alphabet. In Table II, we present the complexity for 16-QAM (in number of real operations) for the proposed MPD, MMSE detector and SUMIS detector with $n_s = 3$. It can be seen that the complexity of the proposed MPD is comparable to/less than MMSE complexity and is less than SUMIS complexity. In addition, the performance of MPD is better than those of MMSE and SUMIS detectors as illustrated below.

| K | Complexity in number of real operations $\times 10^6$ $N = 128$ | | |
|-----|--|---------------|------------------|
| | MMSE | MPD (prop) | SUMIS in [37] |
| 16 | 0.177 | 0.240 | 0.483 |
| 32 | 0.748 | 0.964 | 1.737 |
| 64 | 3.593 | 3.861 | 7.538 |
| 96 | 9.584 | 8.692 | 19.368 |
| 128 | 19.770 | 15.456 | 39.194 |

TABLE II

COMPARISON BETWEEN THE COMPLEXITIES (IN NUMBER OF REAL OPERATIONS) OF THE PROPOSED MPD, MMSE DETECTION, AND SUMIS DETECTION WITH $n_s = 3$ FOR 16-QAM.

Performance: In Fig. 16, we present a comparison between the BER performances of the proposed MPD, MMSE detection, and SUMIS detection with $n_s = 3$, for $N = 128$, $K = 16, 32, 64$, and 16-QAM. A similar comparison between the proposed CHEMP receiver, and the MMSE and SUMIS detectors with MMSE channel estimate is presented in Fig. 17. From these figures, we can see that the proposed MPD outperforms the MMSE and SUMIS detectors under perfect CSI and estimated CSI conditions.

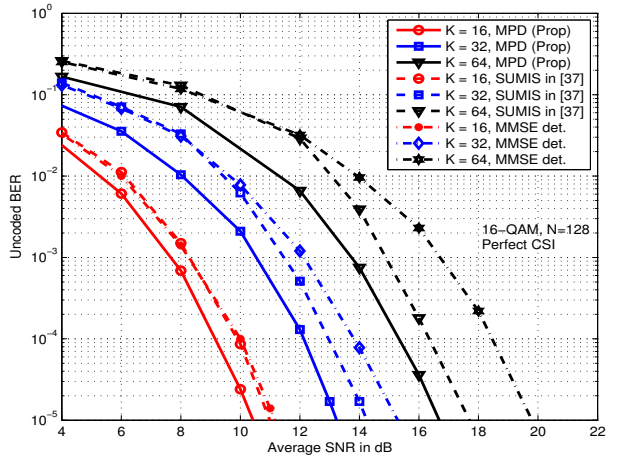


Fig. 16. Comparison of uncoded BER performance of the proposed MPD, MMSE detector and SUMIS detector in [37] with $n_s = 3$ for 16-QAM, $N = 128$, $K = 16, 32, 64$.

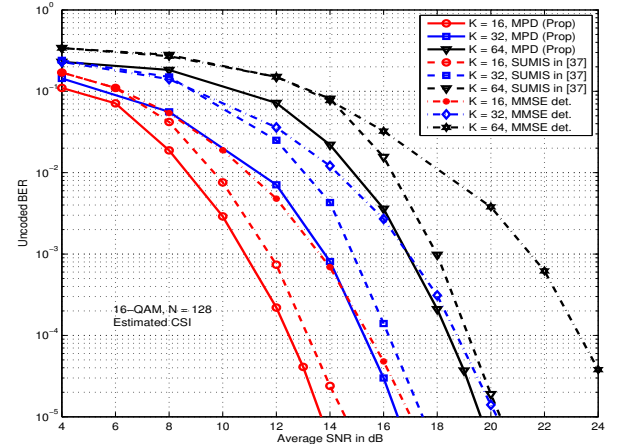


Fig. 17. Comparison of uncoded BER performance of the proposed CHEMP receiver, MMSE and SUMIS detectors with MMSE channel estimate for 16-QAM, $N = 128$, $K = 16, 32, 64$.

VI. DESIGN OF LDPC CODES FOR CHEMP RECEIVER

Since both the proposed CHEMP receiver and the LDPC decoder employ message passing, a detection-decoding approach based on message passing on a joint graph can be natural. In this section, we present a joint graph for the

LDPC coded system model. We perform MPD and LDPC decoding by passing messages on the joint graph. We design optimized irregular LDPC codes specific to the considered large MIMO channel and the CHEMP receiver through EXIT chart matching. We also present the coded BER performance of the LDPC codes thus obtained.

When the detection and decoding operations are performed jointly, the receiver starts the detection-decoding process after receiving n coded bits. In the joint detection-decoding approach, we marginalize the joint probability of the received coded symbols. The objective is to compute

$$\begin{aligned} \Pr(\mathbf{x} | C, \mathbf{y}) &\propto \Pr(\mathbf{x}, C, \mathbf{y}) \\ &= \Pr(C | \mathbf{x}) \Pr(\mathbf{y} | \mathbf{x}) \Pr(\mathbf{x}), \end{aligned} \quad (46)$$

where

$$\Pr(C | \mathbf{x}) = \prod_{l=1}^{n-k} \Pr(C_l | \mathbf{x}), \quad (47)$$

C_l is the event of the l th check equation of the LDPC code being satisfied, and C is the event of all $n-k$ check equations of the LDPC code being satisfied. We formulate a graph whose joint probability factorizes according to (46), and that upon marginalization gives the probability of the transmitted symbols.

A. Joint detector and decoder

Figure 18 shows the joint graph for the LDPC coded large-scale MIMO system with 4-QAM. The joint graph consists of three sets of nodes, namely, variable nodes set, observation nodes set, and check nodes set. The nK observation nodes correspond to the elements of the \mathbf{z} vectors, the nK variable nodes correspond to the transmitted coded symbols over $\frac{n}{2}$ channel uses, and $(n-k)K$ check nodes correspond to the check equations of the LDPC code (see Fig. 18).

Let $i \in \{1, \dots, 2K\}$, $j \in \{1, \dots, K\}$, $m \in \{1, \dots, n\}$, $m' \in \{1, \dots, \frac{n}{2}\}$, and $l \in \{1, \dots, n-k\}$. Now, the different messages passed over the graph are:

- *Observation node $z_i^{m'}$ to variable node s_m^j :* These messages correspond to the probabilities $\Pr(x_i^{m'} = +1)$, the probability of the i th bit transmitted at the $m' = \lceil \frac{m}{2} \rceil$ th channel use, i.e., for a given m' , $m \in \{2m' - 1, 2m'\}$.
- *Variable node s_m^j to check node c_l^j :* These messages correspond to the probabilities $\Pr(b_m^j = +1)$, the probability of the m th bit in the LDPC code block transmitted by the j th user, $l \in \mathcal{N}(s_m^j)$, where $\mathcal{N}(s_m^j)$ is the neighborhood of s_m^j , i.e., the set of all check nodes connected to s_m^j .
- *Check node c_l^j to variable node s_m^j :* These messages correspond to the probabilities $\Pr(C_l^j | s_m^j, \forall r \in \mathcal{N}(c_l^j) \setminus s_m^j)$, where $\mathcal{N}(c_l^j)$ is the neighborhood of c_l^j , i.e., the set of all variable nodes connected to c_l^j . This corresponds to the probability of the l th check

equation of the LDPC code block transmitted by the j th user to be satisfied.

- *Variable node s_m^j to observation node $z_i^{m'}$:*

These messages correspond to the probabilities $\Pr(x_i^{m'} = +1 | C_r^j, x_u^m, \forall r \in \mathcal{N}(s_m^j), u \in \{1, \dots, 2K\} \setminus i)$.

It should be noted that, due to the way messages are defined in the MPD of the CHEMP receiver, there is no message sent from the observation node $z_i^{m'}$ to the variable node $s_{2m'-1}^i$ when $1 \leq i \leq K$, and there is no message sent from the observation node $z_i^{m'}$ to the variable node $s_{2m'}^i$ when $K+1 \leq i \leq 2K$. Similarly, the variable node s_m^j sends no message to any observation node except $z_j^{m'}$ and $z_{2j}^{m'}$. The iterations are continued till all the LDPC check equations are satisfied by the estimated bits or a certain number of iterations are completed.

B. Design of LDPC codes for the joint detector-decoder

We obtain the behavior of the proposed joint detector-decoder through EXIT curve analysis [32]. The EXIT function is $f(I_A) = I_E$, where I_E is the average mutual information between the coded bits and the extrinsic output for a given value of I_A , where I_A is the average mutual information between the coded bits and the input a priori information. First, we obtain the EXIT curves of the CHEMP receiver and combine it with that of the LDPC decoder to obtain the EXIT characteristics of the joint detector-decoder.

The EXIT characteristics of the CHEMP receiver is obtained through Monte Carlo simulations, as an analytical evaluation is intractable. We combine the CHEMP receiver's EXIT curves with those of the LDPC decoder, whose EXIT curves have known closed-form expressions [33]. Figure 19 shows the EXIT curves of the proposed MPD detector and that of the combination of the MPD detector and the variable nodes of the LDPC decoder for 4-QAM, $N = 128$ and $K = 32, 128$. We know that to approach the capacity of the channel using LDPC codes, we need to match the EXIT curves of the check nodes set and the variable nodes set [34], by finding an appropriate degree distribution of the variable nodes and the check nodes that is specific for a channel and receiver. Using the evaluated EXIT curves and the method detailed in [18], we obtain the degree distribution of irregular LDPC codes specific for the large-scale MIMO channel and the proposed CHEMP receiver. The LDPC codes thus obtained for various system parameter settings are presented in Table III.

C. Coded BER performance

We evaluated the coded BER performance of the joint detector-decoder by combining the CHEMP receiver and the LDPC decoder, for $N = 128$ and $K = 16, 32, 64, 96, 128$. Figure 20 shows the coded BER performance of the optimized LDPC codes for the cases with 1) perfect channel

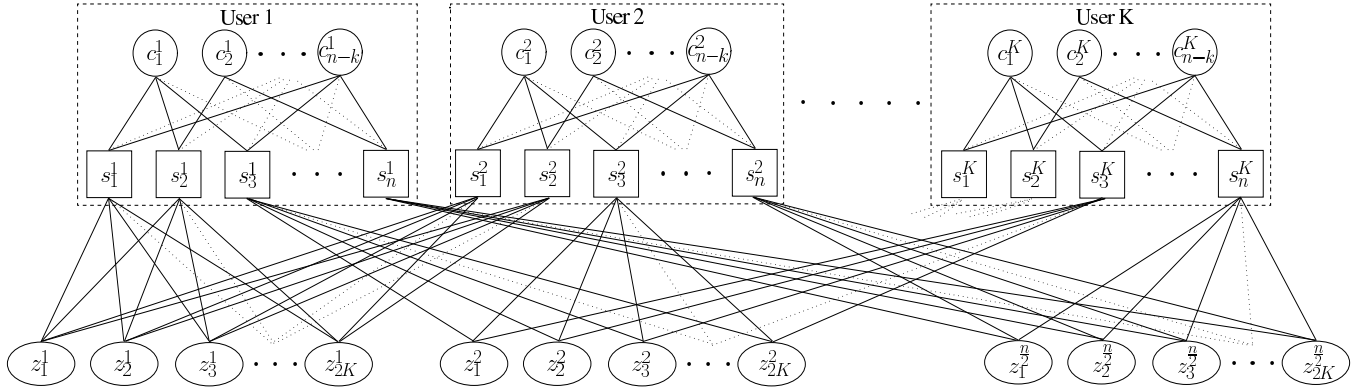


Fig. 18. The joint graph of the LDPC coded large-scale MIMO system.

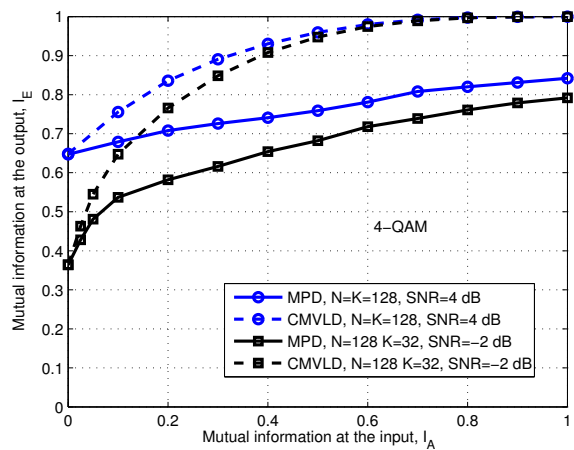


Fig. 19. EXIT curves of 1) proposed MPD, and 2) combination of MPD and variable nodes of the LDPC decoder (CMVLD).

| Parameters | (d_v, p_v) | (d_c, p_c) |
|---------------------------------|--|--|
| $N = 128$, $\alpha = 1$ | $(2, 0.3723), (4, 0.2798),$ $(5, 0.2254), (8, 0.1152),$ $(12, 0.0073)$ | $(6, 0.7067), (12, 0.2531),$ $(18, 0.0402)$ |
| $N = 128$, $\alpha = 0.5$ | $(2, 0.5715), (4, 0.3132),$ $(5, 0.1061), (8, 0.0091)$ | $(4, 0.7045), (8, 0.091)$ $(12, 0.2045)$ |
| $N = 128$, $\alpha = 0.125$ | $(2, 0.4794), (4, 0.4201),$ $(8, 0.0309), (16, 0.0696)$ | $(6, 0.7599), (12, 0.1003)$ $(16, 0.1398)$ |

TABLE III

TABLE III
DEGREE PROFILES OF OPTIMIZED RATE-1/2 LDPC CODES FOR
DIFFERENT LARGE MIMO CONFIGURATIONS. p_v , p_c : FRACTION OF
VARIABLE NODES OF DEGREE d_v AND CHECK NODES OF DEGREE d_c .

knowledge and 2) estimated channel knowledge (i.e., estimated $\mathbf{H}^T\mathbf{H}$), for $N = K = 128$. The minimum SNR required to achieve capacity is also marked. The rate of the LDPC code is 1/2 and the LDPC code block length is $n = 4000$. It can be seen that the optimized LDPC code performs close to within about 3 dB from capacity. We also compare the performance of the optimized codes with that of an off-the-shelf irregular LDPC code from [35]. From Fig. 20, we can see that the optimized LDPC code with perfect channel knowledge performs better than the off-the-shelf

LDPC code by about 1.2 dB at 10^{-5} coded BER. Likewise, the optimized LDPC code with estimated channel knowledge outperforms the off-the-shelf LDPC code by about 0.8 dB.

In Fig. 21, we plot the average SNRs required to achieve a coded BER of 10^{-4} by the optimized LDPC codes with estimated channel knowledge and perfect channel knowledge, as a function of the system loading factor α . From Fig. 21, we observe that the optimized LDPC code with perfect channel knowledge performs better than the off-the-shelf LDPC code in [35] by about 1.2 dB at $\alpha = 1$, and 0.3 dB at $\alpha = 0.125$. Likewise, the optimized LDPC code with the estimated channel outperforms the off-the-shelf LDPC code by about 0.7 dB at $\alpha = 1$, and 0.5 dB at $\alpha = 0.125$. This performance improvement is due to the LDPC code optimization through EXIT curve matching and joint detection-decoding.

In Fig. 22, we show a performance comparison between the proposed optimized code and the codes in [38] and in the WiMax standard [39], in a system with $N = K = 128$, 4-QAM, $n = 11520$, rate-1/2, and perfect CSI. At a block length of $n = 11520$, the proposed optimized code is found to perform close to within about 2.2 dB from capacity. Also, the optimized code is found to perform better than the codes in [38] and [39] by about 2 dB and 2.5 dB, respectively, at 10^{-5} coded BER.

VII. CONCLUSIONS

We proposed a promising message passing based receiver (referred to as the ‘CHEMP receiver’) for low complexity detection and channel estimation in large-scale MIMO systems. The proposed CHEMP receiver is simple and novel (leading to low complexity), yet very effective in large dimensions (leading to near-optimal performance). The key idea is a novel way of exploiting the channel hardening effect that happens in large MIMO channels. Specifically, the receiver worked with approximations to the off-diagonal terms of the $\mathbf{H}^T \mathbf{H}$ matrix, and directly obtained and used an estimate of $\mathbf{H}^T \mathbf{H}$ (instead of an estimate of \mathbf{H}). For the considered large-scale MIMO settings, the proposed message passing detection algorithm has almost the same or less complexity compared

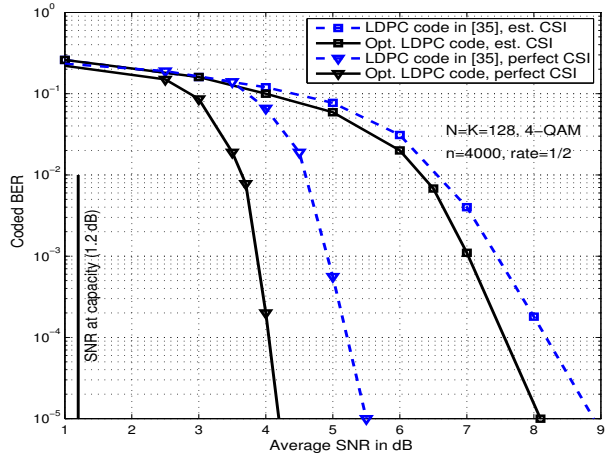


Fig. 20. Coded BER performance of the irregular LDPC codes optimized for the joint detector-decoder with 1) perfect channel knowledge and 2) estimated channel knowledge (i.e., estimated $\mathbf{H}^T \mathbf{H}$), for $N = K = 128$, 4-QAM, $n = 4000$, rate-1/2.

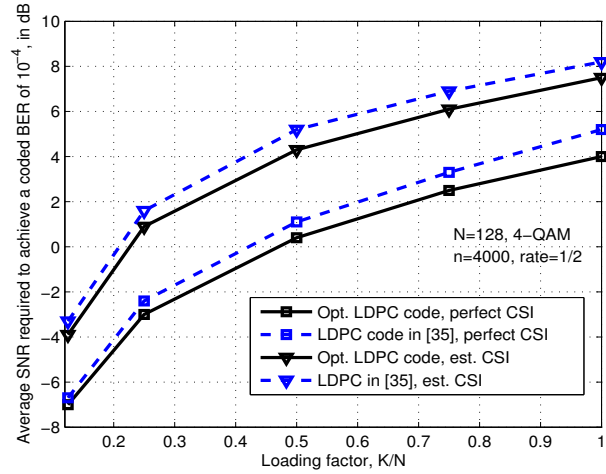


Fig. 21. Comparison of the average SNR required to achieve a coded BER of 10^{-4} by the joint detector-decoder with 1) perfect channel knowledge and 2) estimated channel knowledge (i.e., estimated $\mathbf{H}^T \mathbf{H}$), for various loading factors with $N = 128$, 4-QAM, $n = 4000$, rate-1/2.

to MMSE detection complexity (since the proposed detection algorithm does not need a matrix inversion). Yet, it could achieve much better performance compared to MMSE detection performance. The proposed CHEMP receiver outperformed MMSE and other message passing receivers using an MMSE estimate of \mathbf{H} . We presented an analysis of the convergence of the proposed detection algorithm and a mean square difference analysis of the LLRs in proposed receiver with perfect and estimated CSI. The irregular LDPC codes obtained for the considered large MIMO channel and the proposed CHEMP receiver through EXIT chart matching achieved better coded BER performance compared to off-the-shelf irregular LDPC codes. Stronger conditions for convergence compared to the condition in (28) and convergence

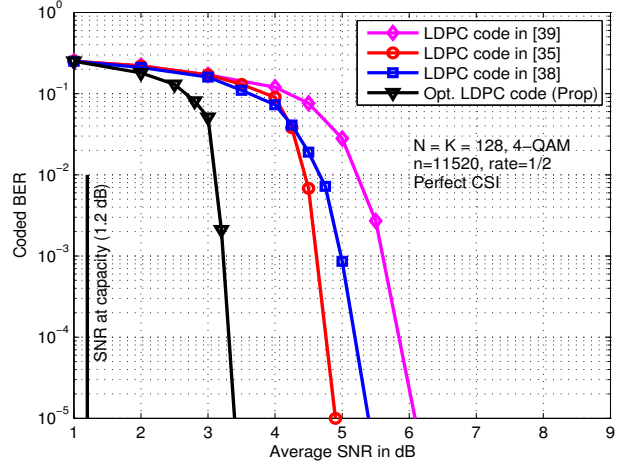


Fig. 22. Coded BER performance comparison between the optimized LDPC code and other LDPC codes in [38] and in WiMax standard [39]. $N = K = 128$, 4-QAM, $n = 11520$, rate-1/2, perfect CSI.

analysis for the case of estimated channel knowledge are potential topics for future research. Extension of the proposed receiver approach to frequency-selective channels can also be carried out as future extension to this work.

REFERENCES

- [1] K. V. Vardhan, S. K. Mohammed, A. Chockalingam, and B. S. Rajan, "A low-complexity detector for large MIMO systems and multicarrier CDMA systems," *IEEE J. Sel. Areas Commun.*, vol. 26, no. 3, pp. 473-485, Apr. 2008.
- [2] S. K. Mohammed, A. Chockalingam, and B. S. Rajan, "A low-Complexity precoder for large multiuser MISO systems," *Proc. IEEE VTC'2008*, pp. 797-801, May 2008.
- [3] S. K. Mohammed, A. Zaki, A. Chockalingam, and B. S. Rajan, "High-rate spacetime coded large-MIMO systems: low-complexity detection and channel estimation," *IEEE J. Sel. Topics Signal Proc.*, vol. 3, no. 6, pp. 958-974, Dec. 2009.
- [4] F. Rusek, D. Persson, B. K. Lau, E. G. Larsson, T. L. Marzetta, O. Edfors, and F. Tufvesson, "Scaling up MIMO: opportunities and challenges with very large arrays," *IEEE Signal Process. Mag.*, vol. 30, no. 1, pp. 40-60, Jan. 2013.
- [5] J. Hoydis, S. ten Brink, and M. Debbah, "Massive MIMO in the UL/DL of cellular networks: how many antennas do we need?" *IEEE J. Sel. Areas in Commun.*, vol. 31, no. 2, pp. 160-171, Feb. 2013.
- [6] B. Cerato and E. Viterbo, "Hardware implementation of a low-complexity detector for large MIMO," *Proc. IEEE ISCAS'2009*, pp. 593-596, May 2009.
- [7] P. Li and R. D. Murch, "Multiple output selection-LAS algorithm in large MIMO systems," *IEEE Commun. Lett.*, vol. 14, no. 5, pp. 399-401, May 2010.
- [8] N. Srinidhi, T. Datta, A. Chockalingam, and B. S. Rajan, "Layered tabu search algorithm for large-MIMO detection and a lower bound on ML performance," *IEEE Trans. Commun.*, vol. 59, no. 11, pp. 2955-2963, Nov. 2011.
- [9] T. Datta, N. Srinidhi, A. Chockalingam, and B. S. Rajan, "Random-restart reactive tabu search algorithm for detection in large-MIMO systems," *IEEE Commun. Lett.*, vol. 14, no. 12, pp. 1107-1109, Dec. 2010.
- [10] C. Knievel, M. Noemm, and P. A. Hoeher, "Low complexity receiver for large-MIMO space time coded systems," *Proc. IEEE VTC'2011-Fall*, pp. 1-5, Sep. 2011.
- [11] P. Som, T. Datta, N. Srinidhi, A. Chockalingam, and B. S. Rajan, "Low-complexity detection in large-dimension MIMO-ISI channels using graphical Models," *IEEE J. Sel. Topics Signal Proc.*, vol. 5, no. 8, pp. 1497-1511, Dec. 2011.

[12] J. Goldberger and A. Leshem, "MIMO detection for high-order QAM based on a Gaussian tree approximation," *IEEE Trans. Inform. Theory*, vol. 57, no. 8, pp. 4973-4982, Aug. 2011.

[13] Q. Zhou and X. Ma, "Element-based lattice reduction algorithms for large MIMO detection," *IEEE J. Sel. Areas Commun.*, vol. 31, no. 2, 274-286, Feb. 2013.

[14] K. A. Singhal, T. Datta, and A. Chockalingam, "Lattice reduction aided detection in large-MIMO systems," *Proc. IEEE SPAWC'2013*, pp. 589-593, Jun. 2013.

[15] T. Datta, N. A. Kumar, A. Chockalingam, and B. S. Rajan, "A novel Monte-Carlo-sampling-based receiver for large-scale uplink multiuser MIMO systems," *IEEE Trans. Veh. Tech.*, vol. 62, no. 7, pp. 3019-3038, Sep. 2013.

[16] P. Svac, F. Meyer, E. Riegler, and F. Hlawatsch, "Soft-heuristic detectors for large MIMO systems," *IEEE Trans. Signal Proc.* vol. 61, no. 18, 4573-4586, Sep. 2013.

[17] L. Dai, Z. Wang, and Z. Yang, "Spectrally efficient time-frequency training OFDM for mobile large-scale MIMO systems," *IEEE J. Sel. Areas Commun.*, vol. 31, no. 2, pp. 251-263, Feb. 2013.

[18] T. Lakshmi Narasimhan, and A. Chockalingam, "EXIT chart based design of irregular LDPC codes for large-MIMO systems," *IEEE Comm. Letters*, vol.17, no.1, pp. 115-118, Jan. 2013.

[19] B. J. Frey, *Graphical Models for Machine Learning and Digital Communication*, Cambridge: MIT Press, 1998.

[20] R. J. McEliece, D. J. C. MacKay, and J-F. Cheng, "Turbo decoding as an instance of Pearls "belief propagation" algorithm," *IEEE J. Sel. Areas Commun.*, vol. 16, no. 2, pp. 140-152, Feb. 1998.

[21] B. M. Kurkoski, P. H. Siegel, and J. K. Wolf, "Joint message-passing decoding of LDPC codes and partial-response channels," *IEEE Trans. Inform. Theory*, vol. 48, no. 6, pp. 1410-1422, Jun. 2002.

[22] D. Bickson, O. Shental, P. H. Siegel, J. K. Wolf, and D. Dolev, "Linear detection via belief propagation," *Proc. 45th Allerton Conf. on Commun., Control, and Comput.*, September, 2007.

[23] B. M. Hochwald, T. L. Marzetta, and V. Tarokh, "Multiple-antenna channel hardening and its implications for rate feedback and scheduling," *IEEE Trans. Inform. Theory*, vol. 50, no. 9, pp. 1893-1909, Sep. 2004.

[24] D. Tse and P. Viswanath, *Fundamentals of Wireless Communication*, Cambridge University Press, 2005.

[25] V. A. Marčenko and L. A. Pastur, "Distribution of eigenvalues for some sets of random matrices," *Math. USSR Sbornik*, vol. 1, pp. 457-483, 1967.

[26] A. Tulino and S. Verdu, *Random Matrix Theory and Wireless Communications*, Foundations and Trends in Communications and Information Theory, Now Publishers, Inc., 2004.

[27] S. Moshavi, E. Kanterakis, and D. Schilling, "Multistage linear receivers for DS-CDMA systems," *Intl. Jl. of Wireless Inform. Netw.*, vol. 3, no. 1, pp. 1-17, Jan. 1996.

[28] J. Hoydis, "Random matrix methods for advanced communication systems," Ph.D. dissertation, Ecole supérieure d'électricité, Gif-Sur-Yvette, France, 2009.

[29] M. Wu, B. Yin, A. Vosoughi, C. Studer, J. R. Cavallaro, C. Dick, "Approximate matrix inversion for high-throughput data detection in the large-scale MIMO uplink," *Proc. IEEE ISCAS'2013*, pp. 2155-2158, May 2013.

[30] A. C. Aitken, "On Bernoulli's numerical solution of algebraic equations," *Proc. Roy. Soc. Edinburgh*, vol. 46, pp. 289-305, 1926.

[31] M. Petti, "A message passing algorithm with damping," *J. Stat. Mech.: Theory and Practice*, Nov. 2005, P11008.

[32] S. ten Brink, "Convergence behavior of iteratively decoded parallel concatenated codes," *IEEE Trans. Commun.*, vol. 49, no. 10, pp. 1727-1737, Oct. 2001.

[33] S. ten Brink, G. Kramer, and A. Ashikhmin, "Design of low-density parity-check codes for modulation and detection," *IEEE Trans. Commun.*, vol. 52, no. 4, pp. 670-678, Apr. 2004.

[34] A. Ashikhmin, G. Kramer, and S. ten Brink, "Extrinsic information transfer functions: A model and two properties," in *Proc. CISS*, Princeton, pp. 742-747, Mar. 2002.

[35] T. Richardson, A. Shokrollahi, and R. Urbanke, "Design of capacity-approaching irregular codes," *IEEE Trans. Inform. Theory*, vol. 47, no. 2, pp. 619-637, Feb. 2001.

[36] J. R. Webb, *Functions of several real variables*, Prentice Hall, 1991.

[37] M. Cirkic and E. G. Larsson, "SUMIS: a near-optimal soft-output MIMO detector at low and fixed complexity," arXiv:1207.3316v2 [cs.IT] 13 Aug 2013.

[38] H. Jilei, P. H. Siegel, and L. B. Milstein, "Performance analysis and code optimization of low density parity-check codes on Rayleigh fading channels," *IEEE J. Sel. Areas in Commun.*, vol. 19, no. 5, pp. 924-934, May 2001.

[39] Air Interface for Fixed and Mobile Broadband Systems, IEEE P802.16e Draft, 2005.